Numerical Simulation of Moisture Swing Absorption Model for Carbon Dioxide Capture

by

Meteb Mejbel

A Thesis Presented in Partial Fulfillment
of the Requirements for the Degree
Master of Science

Approved November 2021 by the
Graduate Supervisory Committee:

Klaus Lackner, Chair
Treavor Boyer
Zhihua Wang

ARIZONA STATE UNIVERSITY

December 2021

ABSTRACT

The current level of carbon dioxide in ambient air is increasing and reinforcing the severity of global warming. Several techniques have been developed to capture the gas directly from the air. Moisture swing absorption (MSA) is a mechanism through which a reactive surface, namely resin beads, absorbs carbon dioxide when dry and releases it when wet. The ionic complexity of the surface of the bead interacts with CO_2 when H_2O contents are low, and CO_2 diffuses as bicarbonate or carbonate. Hence, diffusion-drift-reaction equations describe the moving species behavior MS sorbent. A numerical model has been developed previously applying finite difference scheme (FDS) to estimate the evolution of species concentrations over uniform time and space intervals. The methodology was based on a specific membrane and bead geometry. In this study, FDS was employed again with modifications over the boundary conditions. Neumann boundary condition was replaced by Robin boundary condition which enforced diffusion and drift fluxes at the center of the sorbent. Furthermore, the generic equations were approximated by another numerical scheme, Finite volume scheme (FVS), which discretizes the spatial domain into cells that conserves the mass of species within. The model was predicted to reduce the total carbon mass loss within the system. Both schemes were accommodated with a simulated model of isolated chamber that contained arbitrary sorbent. Moreover, to derive the outcomes of absorption/desorption cycles and validate the performance of FVS, Langmuir curve was utilized to obtain CO_2 saturation in the sorbent and examine two scenarios: one by varying the partial pressure of CO_2 (P_{CO2}) in the chamber at constant H_2O (P_{H2O}), or changing P_{H2O} at constant P_{CO2}. The results from FDS approximation, when adjusting the center with Robin boundary

condition, show 0.11% lower carbon mass gain than when applying Neumann boundary condition. On the other hand, FVS minimizes the mass loss by 0.3% lower than the original total carbon mass and achieves sorbent saturation without any adjustment. Moreover, the isotherm curve demonstrates that increasing P_{H2O} reduces CO_2 saturation and is dependent on the linear and non-linear correlations used to estimate water concentration on the surface.

DEDICATION

I dedicate my work to our beautiful motherland: The Earth. We should give our best to save the planet for ourselves, for the next generations and for the ecosystem. I hope this research would only be the beginning of my work towards fruitful future innovations in sustainability.

ACKNOWLEDGMENTS

I would genuinely like to thank Dr Klaus Lackner for providing the opportunity to work with him, guiding me patiently, and supporting me in this research through tremendous advice. I also want to thank Dr Treavor Boyer and Dr Zhihua Wang for their participation and support to fulfil the work. I would love to thank my wife, Hanine, for her supportive spirit and invaluable advice. I also want to thank Dr Sandip Mazumder, Mr. Ali Akbar Eftekhari, Yusif, Abdulwahab and Fred for their suggestions and technical advice.

TABLE OF CONTENTS

Page

LIST OF FIGURES

LIST OF SYMBOLS

Symbol Page

LIST OF SYMBOLS

Symbol Page

LIST OF SYMBOLS

Symbol Page

CHAPTER 1

INTRODUCTION

Over the last century, environmental concerns have been rising across the world as more environmental issues emerge mainly driven by global warming. Anthropogenic gases that are emitted from multiple sources are continuously piling up in the atmosphere, trapping heat radiating from Earth and warming the planet. As a result, extreme climate events are rising; wildfires and hurricanes are becoming unpredictable and stronger, and humans' quality of life is deteriorating. This led to the Paris Agreement that set a long-term global climate objective to keep the level of temperature increase 1.5˚C to curb the emission (Okia et al., 2018).

Carbon dioxide (CO_2) is one of the primary greenhouse gases that is emitted through human activities and is a major contributor to global warming. CO_2 concentration became substantially high in the air at 400ppm. It is also expected to increase with the increase of energy use of the expanding economy and industrial activities.

Researchers and scientists have been studying CO_2 for many years. They have explored solutions to eliminate the emission of CO_2 and sequestrate it properly. Passive or active methods were determined, and each method has its own cons and pros. Some potential solutions merged from numerous techniques like installing Scrubbers over chimneys, utilizing alternative fuels to produce clean energy, and redesigning chemical processes. Unlike these on-site methods, direct air capture (DAC) is a novel process design that has been developed over years to capture CO_2 directly from ambient air through a number of cycles. Many companies such as Carbon Engineering and Climeworks have already started implementing this process in real life and scaling it up to capture tons of CO_2

daily (Carbon Engineering, n.d.), (Climeworks, n.d.). DAC is composed of a contractor which is mainly reactive sorbents. Their surface is sensitive and selective to the highly diluted concentration of CO_2 in the air. Once the sorbent is fully saturated with the gas, another stage takes place to regenerate the sorbent for another cycle of absorption. These insoluble solids follow a certain technique depending on their molecular structure and polymeric backbone nature to interact with carbon dioxide such as physisorption or chemisorption. Physisorption mechanism happens when a sorbent bonds with the hosted molecule by weak forces such as Van der Waals. On the other hand, chemisorption is when the sorbent binds to the gas through chemical bonding (Berger, Bhown, 2011). Through both mechanisms the sorbent desorbs differently depending on the reactants and products formed after absorption which may be at different temperature or pressure of the surrounding environment and sorbent itself. Lackner and coworkers (2011) has developed a novel mechanism called Moisture swing absorption (MSA) that allows to reduce CO_2 at ambient temperature and pressure. The sorbent captures CO_2 when it is dry and desorbs it when it is wet. The method showed promising results in the uptake rate of the gas and the ability to regenerate in the presence of water at sorbents. The surface of the sorbents (as shown in figure 1.1) is introduced with reactive ions such as hydroxide (OH^-) or carbonate (CO_3^{2-}) on the top surface. To balance the ionic presence over the resin, a counter-ion is attached to the surface of the polymer such as quaternary ammonium (NR_4^+) that interacts with OH^- in one bond or CO_3^{2-} in two bonds.

Remy and Robin have previously developed a theoretical and experimental setup based on moisture swing absorption. Remy (2014) designed a numerical approach to solve for generic simultaneous partial differential equations of reactants and products of MSA.

Forward in time central in space (FTCS) method was accommodated in finite difference scheme (FDS) to solve for partial differential equations in a discretized domain. Two configurations were assumed to implement the models: a flat membrane and a bead. In the membrane, the partial pressure of CO_2 pump mechanism was predicted to occur along the surface. This means one side of the membrane is absorbing CO2 with low moisture and the other side is releasing CO_2 with high moisture content. Robin (2015) established an experimental method to analyze and visualize the effect of moisture on P_{CO2} uptake rate. Additionally, he managed to incorporate a nondimensional simulation procedure to improve the accuracy of the outcomes. To make up for the mass loss in the simulation, due to the non-conservative nature of the scheme used, Robin built carbon conservation generic equation.

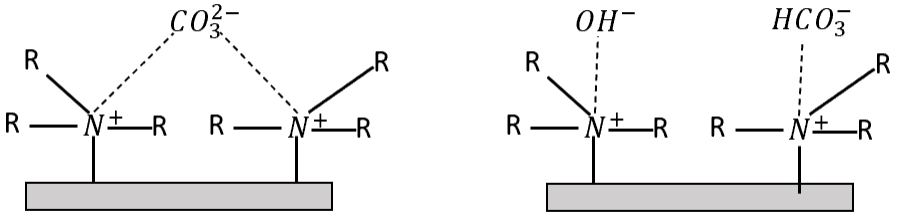

Figure 1.1. Resin Surface Configurations When Treated with CO_3^{2-} or HO^-. The Polymeric Base Serves as the Backbone of the Resin. NR_4^+ is the Counter-ion of the Reactive Ionic Species. R is a Hydrocarbon Species (Lackner et al., 2011).

In this study, previous model was utilized with an additional adjustment that may conserve the mass of the carbon within the system. The scheme can be fixed on the boundaries of the discretized domain to maintain the mass loss. Moreover, finite volume method, known as conservative scheme (FVS) was implemented to examine the temporal-spatial evolution of the species concentration inside the bead and partial

pressure of CO_2 above its surface. It was predicted that the later scheme could offset the carbon mass loss without adjusting the total carbon mass. To test the absorption ability and assumptions in the bead, Langmuir isotherm was employed to obtain CO_2 saturation (θ) in the system. Additionally, two scenarios have been examined to understand the behavior of the bead with carbon and water. In the first scenario, relative humidity of the air is changing inside an isolated chamber while P_{CO2} is kept constant, and vise-versa for the second scenario. The necessity of both scenarios supports the early assumptions in the numerical method. Increasing humidity of the air at constant P_{CO2} perturbs the absorption process of CO_2. On the other hand, increasing P_{CO2} above the surface of the bead could diminish the amount of water inside the sorbent domain. Accordingly, to achieve applicable solutions and more realistic model, a single arbitrary spherical sorbent was assumed inside an isolated chamber that has a specific volume. This can help observe micro changes inside the bead and above its surface within a controlled domain.

The upcoming construction of this paper discusses 4 main chapters. Chapter 2 is a review of the theoretical work on MSA. The presentation will focus on the reactions that take place inside and over the surface of the bead. Also, previous assumptions that were conducted by Remy and Robin are included. Chapter 3 presents the numerical methodology that has been developed along the study to obtain specific results. Chapter 4 discuss the results obtained from the simulation method and how the model evaluation was done. Lastly, chapter 5 summarizes the research and includes suggestions to improve the numerical study in the future.

CHAPTER 2

LITERATURE REVIEW

This section is composed of the theory of moisture swing absorption based on previous work. The introduction explains the behavior of sorbent dealing with dry and wet ambient air. Then previous work of Remy and Robin is illustrated to identify the implemented procedures and assumptions for moisture swing absorption simulation.

2.1 MOISTURE SWING ABSORPTION

Lackner and coworkers (2011) have introduced the ability of certain type of polymeric sorbents that can absorb CO_2 from the ambient air at low moisture conditions. The nature of the resin's surface interacts with CO_2 when it is exposed to dry air or has low humidity level; the surface then desorbs the gas when increasing water content above the surface.[3] Figure 2.1 illustrates the micro process of absorption/desorption cycles above the surface.

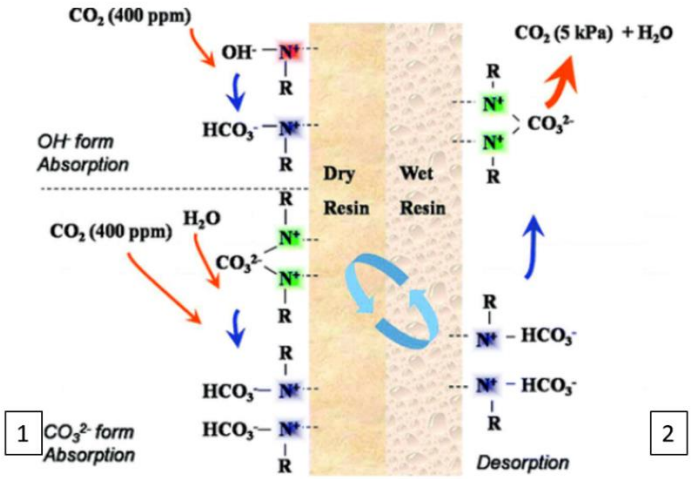

Figure 2.1 Absorption/ Desorption process above the Surface. Packed resins embedded into polypropylene sheet Two stages are pictures: Dry phase with initial presence of either Hydroxide (OH^-) or carbonate (CO^{2-}_3) and Wet phase with fully bicarbonate (HCO_3^-) (Lackner et al., 2011).

In the dry stage, the anions that are the counter ions of the attached cations, which are mainly quaternary ammonium (NR_4^+), play a major role in the reaction with CO_2. The resin can either be fully loaded with OH^- or CO_3^{2-}. Hydroxide phase initializes without carbon presence on the surface (x=0). Hence, as the reaction (reaction 2.1.1) moves forward to produce bicarbonate, x approaches full saturation (x=1) since it is proportionally related the carbon in the system where x is the fractional mass of carbon inside the sorbent.

$$OH^- + C0_2 \overset{K_1}{\leftrightarrow} HCO_3^- \tag{2.1.1}$$

Carbonate phase is another initial stage to begin with. The nature of amine-based anion exchange resin allows the surface to dry spontaneously and shifts the equilibrium reaction (reaction 2.1.2) to the left to form hydroxide and bicarbonate.[3] Therefore, the sorbent intuitively starts absorbing CO2 at half-filled stage (x=0.5).

$$HCO_3^- + HO^- \overset{K_2}{\leftrightarrow} CO_3^{2-} + H_2O \tag{2.1.2}$$

The previous reaction shows the inherent behavior of moisture swing sorbent, and it aligns with Le Chatelier's principle. The water molecules tend to form hydration clouds above the ions which causes the shift if drying or wetting occurs. Moreover, equilibrium constant varies based on the moist presence in the media through an unknown relation (Lackner et al., 2011). In desorption stage, both phases follow the same mechanism for releasing CO_2 from the surface. Reaction 2.1.3 presents the shift from bicarbonate phase to carbonate phase. Hence, the resin will be at the half-filled phase even if it started at the hydroxide phase.

$$2HCO_3^- \rightarrow CO_3^{2-} + H_2O + CO_2 \tag{2.1.3}$$

In short, moisture swing sorbent is derived by equilibrium reactions through which their shift determines which species should be replaced or formed.

2.2: REMY's WORK

To simulate MSA and determine the species' behavior over the resin with different geometries, Remy (2014) established a physical model based on a numerical scheme. The methodology has shown P_{CO2} pump along the membrane geometry and evolution of total carbon mass within spherical beads. Hence, the main assumption was to locate the reaction 2.1.1 and 2.1.2 Figure 2.1.3 visualizes species location within the system. As the CO_2 is above the surface and so reaction $OH^- + C0_2 \overset{K_1}{\leftrightarrow} HCO_3^-$. Then, carbon dioxide diffuses into the system as HCO_3^- and CO_3^{2-} where reaction 2.1.2 occurs in the whole domain. Equilibrium constant of reaction 2.1.2 is dependent on the local humidity, and hence varying water within the shell of membrane or a bead can perturb local equilibria.

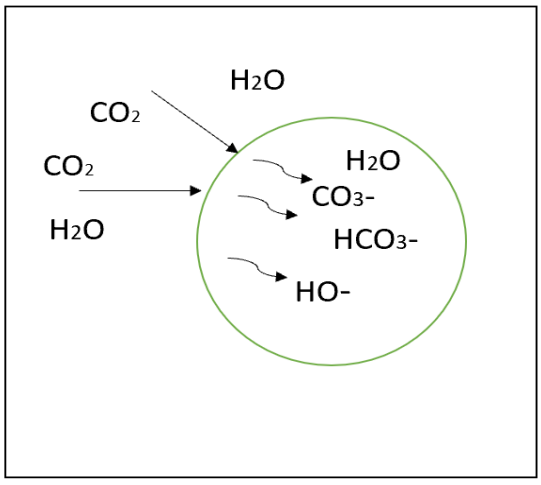

Figure 3.2 A Simple Illustration of species around the bead (which is CO2 and H2O) and Species Diffused Inside the Bead (HO^-, HCO_3^- , CO_3^{2-}, H_2O).[4]

In order to apply the mechanism and satisfy MSA, Remy has managed to consider three main effects that describe the whole process inside the spherical domain. Diffusion is a gradient flux of species' concentration over certain spatial step Δr. Furthermore, as the system holds ionic species, drift current is another flux that generates additional energy to move the species along the spatial domain. Finally, reaction effect, especially reaction 2.2 has to change every time the fluxes impose effect in order to satisfy local equilibrium. Therefore, the mass balance of diffusion-drift- reaction along the whole domain is

$$\frac{\partial C_i}{\partial t} = -[\nabla \mathrm{J_{total}}(\mathrm{r,t}) + \left(\frac{2}{\mathrm{r}}\right)\mathrm{J_{total}}] \pm \beta(\mathrm{r,t}), i = 1, \dots, 4 \qquad (2.2.1)$$

J_{total} is the total flux of diffusion and drift currents, β is the reaction 2.1.2, t is time domain, r is the spatial domain and i is the species index. The concentrations of species are derived through equation 2.2.1 to be accounted at certain distance and time. The ± in the equation represents either reactants or products of species i. J_{total} can be described as,

$$J_{total,i} = J_{diff,i} + J_{drift,i} \qquad (2.2.2)$$

And the diffusion flux is composed of Fick's law,

$$J_{diffusion} = -D_i \frac{dC_i}{dr} \qquad (2.2.3)$$

Where D_i is diffusion coefficient of species i and $\frac{dC_i}{dr}$ is the differential of species concentrations i over radii of sphere. On the other hand, drift flux insists moving ions and the surrounded energy,

$$J_{drift,i} = C_i \mu_i F \qquad (2.2.4)$$

Where μ_i is ionic mobility and F is the electric field which can be $F = -q_i \nabla V$ where q_i is charge of species and ∇V is the electric field that is created by the species. Therefore, the total flux of species i becomes

$$J_{total,i} = -D_i \frac{dC_i}{dr} - \mu_i q_i \nabla V \quad (2.2.5)$$

The underlined equation is known as Nernst-Plank equation which accounts for diffusion and drift fluxes for ions transportation. However, electric field is difficult to determine since you need to validate the effect of 3 neighboring ionic species. Hence, Remy assumed the sum of all species is null,

$$J_{total} = J_{HCO_3^-} + J_{HO^-} + 2J_{CO_3^{2-}} = 0 \quad (2.2.6)$$

Then applying eq 2.2.5 for each ionic compound into the null equation to achieve a reliable solution of ∇V. Hence, null equation becomes

$$J_{d,HCO_3^-} + J_{d,OH^-} + 2J_{d,CO_3^{2-}} + \nabla V\left(C_{HO^-}\mu_{OH^-} + C_{HCO_3^-}\mu_{HCO_3^-} + 4C_{CO_3^{2-}}\mu_{CO_3^{2-}}\right) = 0 \quad (2.2.7)$$

Which then electric field can be solved into

$$\nabla V = -\frac{J_{d,HCO_3^-} + J_{d,OH^-} + 2J_{d,CO_3^{2-}}}{\left(C_{HO^-}\mu_{OH^-} + C_{HCO3^-}\mu_{HCO3^-} + 4C_{CO3^{2-}}\mu_{CO3^{2-}}\right)} \quad (2.2.8)$$

The electric field correlation had been identified, thanks to Robin.[5] The absence of water was noticed from previous relationship due its neutrality. To sum up all the equations into a useful model, Remy had created other assumptions to simulates the nature of MSA. The initial concentrations of all species along r were known and at global equilibrium. At t=0, accommodating with either P_{CO2} or relative humidity (RH), the system becomes out of equilibrium where all molecules redistribute inside the whole bead. Furthermore, it was assumed that the rate of diffusion and drift are lower than the equilibrium rate. Hence, the process was divided into two steps; a step where species travel through spatial and

temporal intervals and another step when they are forced to come back to local equilibrium.

$$C_i(r_j, t_m) \xrightarrow{diffusion+drift} C_i(r_j + \Delta r, t_m + \Delta t) \xrightarrow{reaction} C_i(r_j + \Delta r, t_m + \Delta t) \quad (2.2.9)$$

Where j and m are space and time index respectively along the domain of r and t. The previous underlined process consists of two steps; first the concentration of species i transports temporally and spatially at specific space and time interval, then the local concentration is adjusted to satisfy equilibrium reaction. That is, reaction 2.1.2 must be instantaneously fast to reach equilibrium at a certain space. Therefore, the total flux equations for species HO^-, HCO_3^-, CO_3^{2-} and water are

$$J_{tot,HO^-} = J_{d,HO^-} + C_{OH^-}\mu_{HO^-}\frac{J_{d,OH^-} + J_{d,HCO_3^-} + 2J_{d,CO_3^{2-}}}{C_{OH^-}\mu_{OH^-} + C_{HCO_3^-}\mu_{HCO_3^-} + 4C_{CO_3^{2-}}\mu_{CO_3^{2-}}} \quad (2.2.10)$$

$$J_{tot,HCO_3^-} = J_{d,HCO_3^-} + C_{HCO_3^-}\mu_{HCO_3^-}\frac{J_{d,OH^-} + J_{d,HCO_3^-} + 2J_{d,CO_3^{2-}}}{C_{OH^-}\mu_{OH^-} + C_{HCO_3^-}\mu_{HCO_3^-} + 4C_{CO_3^{2-}}\mu_{CO_3^{2-}}} \quad (2.2.11)$$

$$J_{tot,CO_3^{2-}} = J_{d,CO_3^{2-}} + 2C_{CO_3^{2-}}\mu_{CO_3^{2-}}\frac{J_{d,OH^-} + J_{d,HCO_3^-} + 2J_{d,CO_3^{2-}}}{C_{OH^-}\mu_{OH^-} + C_{HCO_3^-}\mu_{HCO_3^-} + 4C_{CO_3^{2-}}\mu_{CO_3^{2-}}} \quad (2.2.12)$$

$$J_{tot,H_2O} = J_{d,H_2O} \quad (2.2.13)$$

The fluxes can be implemented into equation 2.2.1 which corresponds to each species. Hence, the results of applying 4 special fluxes are 4 generic partial differential equations (PDEs) that can be solved via a numerical scheme (finite difference method) and then the reaction can be evaluated separately.

To obtain a numerical solution, the boundaries at the edge of each domain have to be identified, knowing that the gradients evolution are bounded between edge of the bead r=R where R is the radius of the bead and the center (r=0). Remy's estimated that the

reaction $OH^- + C0_2 \overset{K_1}{\leftrightarrow} HCO_3^-$ occurs at the edge of the bead R where the consumption of CO2 is taking place. Then the equilibrium expression can be expressed by the relationship between the equilibrium constant and the concentrations of the reactants and products.

$$K_1 = \frac{C_{HCO_3^-}}{C_{OH^-} C_{CO_2}} \tag{2.2.14}$$

The equilibrium concentration of CO_2 can be found via Henry's law which is a linear correlation between the P_{CO2} above the surface and C_{CO2} on the surface.

$$C_{CO_2} = H_{CO_2} P_{CO_2} \tag{2.2.15}$$

Where H_{CO2} is Henry's constant. Another equation which appears at the whole domain of the bead (0<r<R) is reaction $HCO_3^- + HO^- \overset{K_2}{\leftrightarrow} CO_3^{2-} + H_2O$ knowing that K_2 is dependent on the local moisture content and hence equilibrium expression be

$$K_2 = \frac{C_{CO_3^{2-}} C_{H_2O}}{C_{OH^-} C_{HCO_3^-}} = k\left(C_{H_2O}\right)^p \tag{2.2.16}$$

Where k and p are isotherm parameters that can be assumed based on the conditions that were applied to obtain the equilibrium reaction at the whole domain. As water concentration appears in the previous expression, there should be a validated correlation to determine C_{H2O} on the surface of the resin and P_{H2O} above. Therefore, Remy assumed a linear relationship between P_{H2O} above the surface of the bead and C_{H_2O} inside the resin using linear correlation which states

$$C_{H_2O} = k_{H_2O} P_{H_2O} \tag{2.2.17}$$

Although, this relationship is not true all the time especially in the polymer absorption process which will be described later in the report. To combine all the previous

expressions used on the boundary R, electroneutrality was assumed (adds all the ions and cations in the system). The only counter-ion known in the system is quaternary ammonium. Then, electroneutrality becomes

$$C_{OH^-} + C_{HCO_3^-} + 2C_{CO_3^{2-}} = C_{NR_4^+} \tag{2.2.18}$$

Since all expressions have been identified on the surface, the unknown concentrations can be obtained since there are 4 equations and 4 unknowns which are $C_{HO^-}, C_{HCO_3^-}, C_{CO_3^{2-}}$ and C_{H_2O}. The movement of the species molecules was restricted at the center of the domain. Hence, the diffusion fluxes at the center were zero at all times.

$$\frac{dC_i}{dr}(0,t) = 0 \tag{2.2.19}$$

Thus, the boundary at the center is Neumann flux. Both boundaries were identified so the numerical scheme could be implemented for further study of species behavior inside the bead. Remy assumed that all concentrations were known at t=0, then to find the concentrations of species i at the whole domain, time derivative was solved explicitly, and the domain was divided into shells so that C_i at t=t+1 was expressed as

$$C_i(r_j, t_{m+1}) = C_i(r_j, t_m) - \Delta t\left[\nabla J(r_j, t_m) + \frac{2}{r}J(r_j, t_m)\right] \pm \beta(r_j, t_{m+1}) \tag{2.2.19}$$

Where j and m are space and time index, respectively. β is the local equilibrium reaction 2.1.2 term at r_j and obtained instantaneously at t_m=t+Δt.

$$K_2 C_{CO_3^{2-}}(r_j, t_{m+1}) C_{H_2O}(r_j, t_{m+1}) - C_{HO^-}(r_j, t_{m+1}) C_{HCO_3^-}(r_j, t_{m+1}) = 0 \tag{2.2.20}$$

Where all equilibrium concentrations of species HO^-, HCO_3^-, CO_3^{-2} and H_2O were determined numerically via equilibrium constant, conversation expression and initial concentrations of the prospective species at r_j.

The numerical scheme that Remy has imposed was finite difference scheme (FDS). FDS approximates the derivative of dependent variables over independent or controlled parameters such as space or time. The study herein was accounted solely for radii dimension which was one dimensional range. Hence, the spatial range from r=0 to r=R was divided evenly by distance step Δr and formed number of nodes at each r_j over domain R.

$$r_j = (j-1)\Delta r \qquad (2.2.21)$$

Where j=1, …, S. S is the total number of nodes. Then, spatial step can be estimated by $\Delta r = \frac{R}{S}$. At every node inside, HO^-, HCO_3^-, CO_3^{2-} and H_2O appear at the same space. However, the species are not restricted at the same spot, the flux gradients create an internal motion. Therefore, time interval was added to determine the concentrations at next time step tm.

$$t_m = (m-1)\Delta t \qquad (2.2.22)$$

Where m is the number of time intervals m=1, …, M, then time step can be estimated by $\Delta t = \frac{t}{M}$. Consequently, the time and space domain were cut into number of space and time nodal portions as shown in figure 3.1. thereby, the nodes make a gradient boundary by itself and hence the mass balance equation 2.2.19 is applicable over the nodes to be demonstrated.

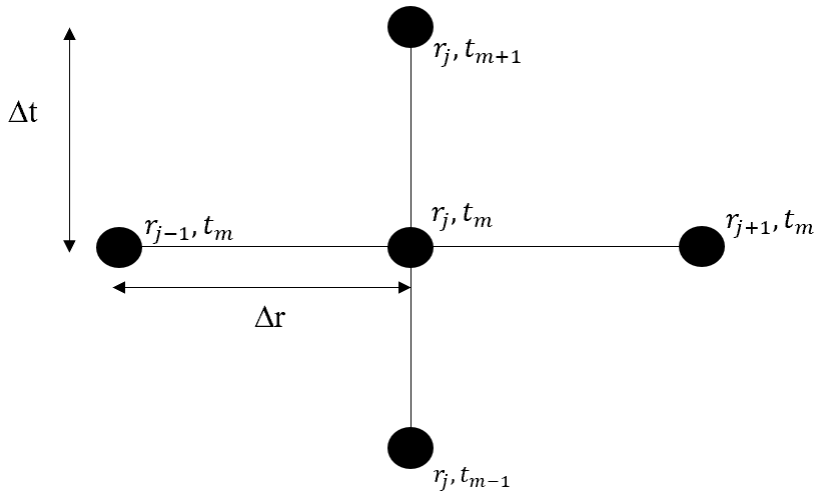

Figure 2.3 Internal spatial Nodes. The nodes are divided by space and time step. North and south nodes are temporal change end east and west are the spatial change.

From the previous illustration, the discretized model of 1-dimansional spherical space that holds species concentration C_i can be approximated via FDS. With the prospective scheme, the accuracy varies based on the size of controlled parameters. Longer space or time steps often increase the fluctuation of the solution at and hence lower accuracy. To manage the accuracy, the suggestion was made on the controlled factor that must be $0.5 \geq D_i \frac{\Delta t}{\Delta r^2}$=G. The unitless factor should not exceed 0.5 since the scheme is conditionally stable.

The scheme could be derived through either implicit or explicit solutions. The difference relies on number of unknown dependent variables to be solved. Implicit solution has higher number of unknown variables (at next time step). In explicit method, only one variable should be solved at next time step and depends on the initial variables. In comparison to explicit solution, implicit has higher order of accuracy than explicit which induces the condition that unitless G term has to be less or equal to 0.5.

Forward in time, center at space (FTCS) is one of the explicit finite difference schemes. Generally, the partial differential equations were derived into time and space derivative. As the phrase explains itself, time derivative was solved in next time step $t_m+\Delta t$. Hence the concentration of species i as first order time dependent became

$$\frac{\partial C_i(r_j, t_m)}{\partial t} = \frac{C_i(r_j, t_m + 1) - C_i(r_j, t_m)}{\Delta t} \tag{2.2.23}$$

And concentration of species i as space dependent variable was evaluated into first and second order based on the neighboring spatial nodes thanks to Taylor's expansion method.

$$\frac{\partial C_i(r_j, t_m)}{dr} = \frac{C_i(r_j + 1, t_m) - C_i(r_j - 1, t_m)}{\Delta r} \tag{2.2.24}$$

$$\frac{\partial^2 C_i(r_j, t_m)}{\partial r^2} = \frac{C_i(r_j + 1, t_m) - 2C_i(r_j, t_m) + C_i(r_j - 1, t_m)}{\Delta r^2} \tag{2.2.25}$$

Therefore, PDE equations (eq 2.2.1) for each species on a prospective j node can be solved numerically. At $t=t_m$ all concentrations are known and at $t=t_m+\Delta t$ the species are out of equilibrium and fluxes causing motion around adjacent nodes. Accordingly, the fluxes were solved in the first place then reaction obtained as expected to experience fast rate of reaction. MATLAB was utilized as a simulator tool to conduct the model.

2.3: ROBIN's WORK

Robin (2015) continued the numerical simulation built by Remy and combined it with experimental setup to evaluate his findings. The numerical analysis was redesigned into a dimensionless analysis for the purpose of simplifying the model. The variance between

unitless and actual variables was controlled by global parameters such as the pressure of the system, cation concentration and water diffusion coefficient. Furthermore, Robin re-evaluated critical parameters to accommodate his numerical simulations. For example, the concentration of cations inside the bead as the manufacturer provided was 2095mol/m^3. Robin constructed a titration experiment to obtain the actual cation concentration which was 1620mol/m^3. The equilibrium constants values were determined based on the conditions that the membrane was tested on. And the temporal-spatial evolution of species' concentration inside the membrane sheet was obtained and P_{CO2} pump at specific conditions was proven.

Additionally, Robin calculated and measured the partial pressure of CO_2 of the system during adsorption/desorption process. Theoretically, P_{CO2} above the surface of the bead is changing over time with varying P_{H2O}. Therefore, he identified a relationship between the total amount of carbon inside and outside the beads.

The only known parameters which can be utilized by Robin were P_{CO2}, P_{H2O} and pressure of the whole system. Given the controlled parameters within a controlled volume (V_{system}) and the total carbon mass inside the bead (HCO_3^- and CO_3^{2-}), two methods were conducted to solve P_{CO2} at next time step: carbon conservation and flux extrapolation. Flux extrapolation determines the total carbon flux ($J_{d,HCO_3^-} + J_{d,CO_3^{2-}}$) from the bead to the air. On the other hand, carbon conservation estimates total carbon mass inside the bead and calculates gain and loss of carbon from P_{CO2}. Accordingly, the total carbon mass inside a controlled system $n_{total\ carbon}$ can be obtained by equation 2.3.1.

$$n_{tot\_C} = \sum_{j=1}^{j} \left(\frac{\Delta C_{HCO_3^-}^{r_{j+1}} + \Delta C_{HCO_3^-}^{r_j}}{2} + \frac{\Delta C_{CO_3^{2-}}^{r_{j+1}} + \Delta C_{CO_3^{2-}}^{r_j}}{2} \right) V_{shell} + \frac{P_{CO_2}}{R_i T} V_{air} \qquad (2.3.1)$$

Where R_i is ideal gas constant (R_i=8.206*10^{-6}atm*m^3*K^{-1}*mol^{-1}), T is temperature of the surrounding, V_{shell} is partial volume of each shell in the bead and V_{air} is volume of the air. Also, the average of internal carbon can be determined through equations 2.3.2, 2.3.3, 2.3.4 and 2.3.5

$$\Delta C_{HCO_3^-}^{r_{j+1}} = C_{HCO_3^-}(r_{j+1}, t_{m+1}) - C_{HCO_3^-}(r_{j+1}, t_m) \qquad (2.3.2)$$

$$\Delta C_{CO_3^{2-}}^{r_{j+1}} = C_{CO_3^{2-}}(r_{j+1}, t_{m+1}) - C_{CO_3^{2-}}(r_{j+1}, t_m) \qquad (2.3.3)$$

$$\Delta C_{HCO_3^-}^{r_j} = C_{HCO_3^-}(r_j, t_{m+1}) - C_{HCO_3^-}(r_j, t_m) \qquad (2.3.4)$$

$$\Delta C_{CO_3^{2-}}^{r_j} = C_{CO_3^{2-}}(r_j, t_{m+1}) - C_{CO_3^{2-}}(r_j, t_m) \qquad (2.3.5)$$

So, in order to evaluate P_{CO2} above the surface at time step Δt, 2.3.1 has been rearranged as follows

$$P_{CO_2}^{t_m+1} = P_{CO_2}^{t_m} - \frac{R_i T}{V_{air}} \sum_{j=1}^{j} \left[\left(\frac{\Delta C_{HCO_3^-}^{r_{j+1}} + \Delta C_{HCO_3^-}^{r_j}}{2} + \frac{\Delta C_{CO_3^{2-}}^{r_{j+1}} + \Delta C_{CO_3^{2-}}^{r_j}}{2} \right) V_{shell} \right] \qquad (2.3.6)$$

Where $P_{CO_2}^{t_m+1}$ is partial pressure of CO_2 at next time step and $P_{CO_2}^{t_m}$ is the initial P_{CO2}.

Equation 2.3.6 was utilized in the recent study to calculate P_{CO2} at other assumptions.

CHAPTER 3

THEORETICAL AND NUMERICAL METHODOLOGY

The following section covers the steps taken to numerically simulate moisture swing absorption generic model. Each subsection incorporates the assumptions made and the equations utilized to manage a sophisticated numerical model and find approximated results.

3.1: FINITE DIFFEENCE SCHEME: NULL FLUXES AT CENTER BOUNDARY CONDITION

The scheme was conducted again with the same procedure that was employed by Remy in order to detect the difference between the assumptions she made at the center and this model. As mentioned in the previous section, the flux at the center is null, and thus no transportation occurs beyond the center point. However, diffusion flux was solely applied at the center which neglected the effect of drift flux. Hence, FDS was reconstructed at the center to be applied over the spherical domain with respect to a new boundary condition (BC). Although, the mass varies along r distance and θ and φ angles, the approximation was made using one dimensional domain for the purpose of simplicity and consistency with the previous model made by Remy. Hence, the spatial and temporal division technique remained the same in this study where r=0 to r=R for r_j=1, …, S and t=0 to t=t for t_m=1, …, M. Moreover, the explicit method was utilized to comply with the previous simulation.

To make the internal nodes susceptible to change, the boundary conditions must be satisfied. When r=R, the surface is exposed to varying P_{CO2} and P_{H2O} in the surrounding. Hence, constant concentrations were assumed at the boundary node *j*=S (Dirichlet BC).

$$C_i(S, t_m) = C_{i,surface}\,, \qquad t_m = 1, \dots, M \tag{3.1.1}$$

Where $C_{i,surface}$ is the equilibrium concentration of species i that was estimated based on the species relationship in the surface. On the other side of the spatial domain, no concentration gradient is present beyond the center which restricts molecular motion. Deriving an approximated expression for the internal node j=1, given that the examined geometry was spherical bead, would lead to indeterminant solution since $r_j=(j-1)\Delta r$. Therefore, L'Hospital's rule was used to find r in the denominator.

$$\lim_{r\to 0} \nabla J_{i,tot} + \frac{2}{r} J_{i,tot} = \nabla J_{i,tot} + 2\nabla J_{i,tot} = 3\nabla J_{i,tot} \tag{3.1.2}$$

Remy derived the radii derivative assuming there was a fictitious node on the other side of the spatial interval to apply Neumann BC. Figure 3.2 illustrates the nodes' configuration at the center. Then the first and second order of concentration derivative can be roughly obtained with respect to zero diffusion flux at j=1.

$$\frac{dC_i(1, t_m)}{dr} = \frac{C_i(2, t_m) - C_i(0, t_m)}{\Delta r} = 0 \tag{3.1.3}$$

$C_i(0, t_m)$ was substituted by $C_i(2, t_m)$ then implemented in the second derivative approximation.

$$\frac{d^2C_i(1, t_m)}{dr^2} = \frac{2[C_i(2, t_m) - C_i(1, t_m)]}{\Delta r^2} \tag{3.1.4}$$

A correlation at the center can then be applied at all the time.

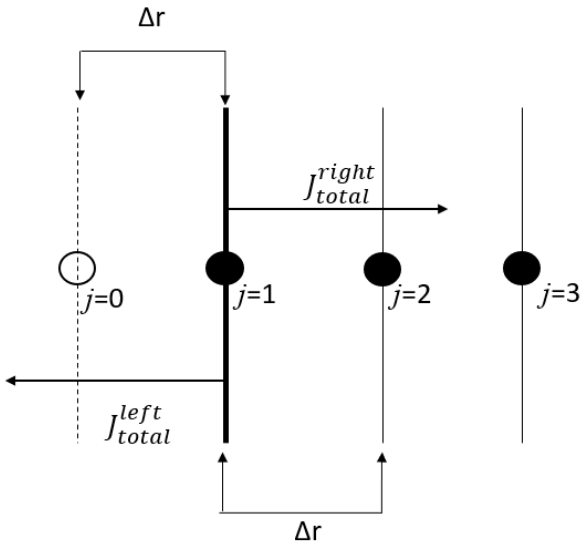

Figure 3.1 Schematic of Spatial Node at the Center of the Bead. As shown, the fictitious point at j=0 is on the left side of the domain (outside of the tested intervals). Node j=1 is located at the boundary. FD scheme is bounded by the boundary conditions as part of the discretized domain.

However, Neumann BC is significant for solely one flux at t_m which was diffusion based in Remy's simulation. Yet, the molecules at the center experience two effects: diffusion and drift. Therefore, Robin BC was prioritized instead of Neumann to incorporate both fluxes, knowing that $J_{total,i} = J_{diffusion,i} + J_{drift,i}$, then, $J_{total,i} = 0$. Moreover, the backward fluxes $J_{total,i}^{j-1}$ was assumed to be null at j=1 to avoid mass loss or gain of internal concentration of species and satisfy mass conservation of the whole system. Then Robin BC was integrated into a useful function with initial known concentrations.

$$J_{tot,HO^-} = -D_i \frac{dC_i}{dr} - q_i C_i \mu_i \frac{J_{diff,HO^-} + J_{diff,HCO_3^-} + 2J_{diff,CO_3^{2-}}}{C_{HO^-}\mu_{HO^-} + C_{HCO_3^-}\mu_{HCO_3^-} + 4C_{CO_3^{2-}}\mu_{CO_3^{2-}}} = 0 \quad (3.1.5)$$

Where D_i and μ_i for all species were kept constant to avoid nonlinearity. In fact, the total flux applies for all ionic species except water which is neutral. The function could be solved simultaneously through iteration at each node, but it would be expensive numerically. Fortunately, with explicit scheme and known concentration at $t=t_m$, other

concentrations could be held constant even though the change continues occurring over the domain [0,R].

To examine the validity of the new boundary condition applied at the center, the FD was simulated through MATLAB to obtain the temporal-spatial process of diffusion-drift-reaction approximated equations and analyze the behavior inside the bead. Also, P_{CO2} changing over the surface was another factor that was tested to determine the global carbon conversation when applying Neumann and Robin boundary conditions. Consequently, equation 2.3.1 was incorporated at each time step to manually adjust the mass loss or gain of the system.

3.2: FINTIE VOLUME METHOD: MASS CONSERVATIVE SCHEME

Controlling mass conservation through a number of numerical solutions could be complex since it is highly subject to mass conservation inaccuracy. Numerical schemes should either be modified manually, like in the previous FDM scheme, or imposed by a highly iterative model. There are other numerical structures that feature mass conservation of dependent variables within a certain domain. Finite volume method (FVM) is a discretized scheme that approximates derivative forms through a specific size of volume intervals (v_a). Hence, the mass at that point becomes the average over distance Δr and converges at an averaged solution (Mazumder, 2016, p.277).

3.2.1: FINITE VOLUME SCHEME INTERNAL SEGMENTS

The discretized FDS intervals inside the bead [0, R] are reformed into a number of v_a intervals as shown in figure 3.2. The nodes are relocated inside a cell, namely v_a, over Δr between a left and a right boundary [$v_{a,L}$, $v_{a,R}$] (constant size over domain [0, R]); unlike FDS, which enforces the nodes to be located at 1-d boundaries.

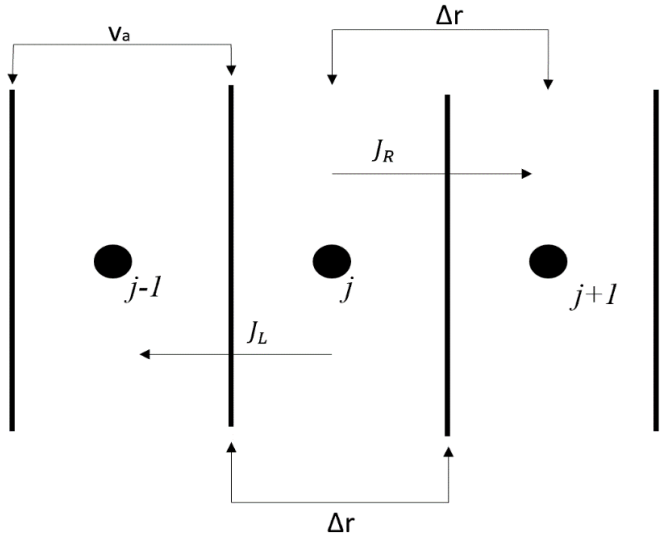

Figure 3.2 Schematic of Discretized Internal Nodes with interval v_a Based on Finite volume method. The fluxes cross the boundaries at the left and right side.

The fluxes are also averaged in the FV scheme since the concentration gradients of the species are within v_a and are moving in both directions. Hence, PDE 2.2.1 was reconstructed into a canonical form

$$\frac{\partial \bar{C}_i}{\partial t} = -[\nabla \bar{J}_{\text{total}}(\mathrm{r_j}, \mathrm{t_m}) + \left(\frac{2}{\mathrm{r_j}}\right)\bar{J}_{\text{total}}(\mathrm{r_j}, \mathrm{t_m})] \pm \bar{\beta}(\mathrm{r_j}, \mathrm{t_m}) \qquad (3.2.1)$$

Where $\bar{J}_{tot,i}$, $\bar{C}_i$ and $\bar{\beta}$ are the averaged flux, concentration and reaction over $v_{a,L}$ to $v_{a,R}$, respectively. For simplicity, $J_{tot,i}, C_i$ and r will replace the average script terms for the rest of the paper. The total fluxes were then determined to the left and right directions.

For $\nabla J_{\text{total}}(\mathrm{r_j}, \mathrm{t_m})$, the gradient script was integrated over the volume v_a, where node j is located.

$$\nabla J_{\text{tot}}(\mathrm{r_j}, \mathrm{t_m}) = \frac{J_{\text{tot,R}}(\mathrm{r_j}, \mathrm{t_m}) - J_{\text{tot,L}}(\mathrm{r_j}, \mathrm{t_m})}{\Delta r} \tag{3.2.2}$$

Whereas $J_{\text{tot}}(\mathrm{r_j}, \mathrm{t_m})$ was linearly averaged since the term is not enforced with a gradient term.

$$J_{\text{tot}}(\mathrm{r_j}, \mathrm{t_m}) = \frac{J_{\text{tot,R}}(\mathrm{r_j}, \mathrm{t_m}) + J_{\text{tot,L}}(\mathrm{r_j}, \mathrm{t_m})}{2} \tag{3.2.3}$$

The equation of total flux of species i is composed of several first order derivatives of C_i that are stored in cell v_a. Then, every derivative can be approximated to the left and right side of the cell boundary [$v_{a,L}$, $v_{a,R}$].

$$\left(\frac{\partial C_i}{\partial r}\right)_L = \frac{C_i(r_j, t_m) - C_i(r_{j-1}, tm)}{\Delta r} \tag{3.2.4}$$

$$\left(\frac{\partial C_i}{\partial r}\right)_R = \frac{C_i(r_{j+1}, t_m) - C_i(r_j, tm)}{\Delta r} \tag{3.2.5}$$

Diffusion coefficients and ionic mobility of species i are susceptible to be averaged over the cell boundaries. However, in the recent study, both coefficients were constant over the boundary of each cell. The denominator of $J_{\text{drift,i}}(\mathrm{r_j}, \mathrm{t_m})$ shows concentration variables of species HO^-, HCO_3^- and CO_3^{2-}. So, they were averaged linearly to satisfy the scheme. Thus, the approximated terms were rearranged into $J_{\text{drift,R}}$ and $J_{\text{drift,L}}$.

$$J_{\text{drift,R}}(\mathrm{r_j}, \mathrm{t_m}) = \frac{\mu_i\left(C_{i,r_{j+1}}^{t_m} - C_{i,r_j}^{t_m}\right)}{\Delta r} \frac{\left(\mu\left(C_{i,r_{j+1}}^{t_m} + C_{i,r_j}^{t_m}\right)_{HO^-} + \mu\left(C_{i,r_{j+1}}^{t_m} - C_{i,r_j}^{t_m}\right)_{HCO_3^-} + 2\mu\left(C_{i,r_{j+1}}^{t_m} - C_{i,r_j}^{t_m}\right)_{CO_3^{2-}}\right)}{\mu\left(C_{i,r_{j+1}}^{t_m} + C_{i,r_j}^{t_m}\right)_{HO^-} + \mu\left(C_{i,r_{j+1}}^{t_m} + C_{i,r_j}^{t_m}\right)_{HO^-} + 4\mu\left(C_{i,r_{j+1}}^{t_m} + C_{i,r_j}^{t_m}\right)_{CO_3^{2-}}} \tag{3.2.6}$$

$$J_{\text{drift,L}}(\mathrm{r_j}, \mathrm{t_m}) =$$

$$\frac{\mu_i \left(C_{i,r_j}^{t_m} - C_{i,r_{j-1}}^{t_m}\right)}{\Delta r} \frac{\left(\mu \left(C_{i,r_j}^{t_m} + C_{i,r_{j-1}}^{t_m}\right)_{HO^-} + \mu \left(C_{i,r_j}^{t_m} - C_{i,r_{j-1}}^{t_m}\right)_{HCO_3^-} + 2\mu \left(C_{i,r_j}^{t_m} - C_{i,r_{j-1}}^{t_m}\right)_{CO_3^{2-}}\right)}{\mu \left(C_{i,r_j}^{t_m} + C_{i,r_{j-1}}^{t_m}\right)_{HO^-} + \mu \left(C_{i,r_j}^{t_m} + C_{i,r_{j-1}}^{t_m}\right)_{HO^-} + 4\mu \left(C_{i,r_j}^{t_m} + C_{i,r_{j-1}}^{t_m}\right)_{CO_3^{2-}}} \quad (3.2.7)$$

Since all terms were approximated over cell v_a for grid point j, equation 3.2.1 was rearranged to determine the flux knowing that the time derivative was obtained explicitly, and the reaction could then be solved at end of $t_m+\Delta t$. The FV scheme is stable because G can be modified with no restrictions especially with size Δr or Δt. The solution, however, may diverge if the initial concentrations are not carefully estimated. In order to estimate Δr and Δt, equation 3.2.8 and 3.2.9 were applied.

$$r_j = j\Delta r, \qquad for\ j = 1, \dots, S \quad (3.2.8)$$

$$t_m = (m-1)\Delta t \quad for\ m = 1, \dots, t+1 \quad (3.2.9)$$

3.2.2: FINITE VOLUME METHOD BOUNDARY CONDITIONS

After the internal segments were identified with numerical expressions, the edge and the center of the sorbent had to be specified to finalize the numerical scheme. In the FD scheme, nodes j=1 is located at the center and j=S is located at the surface of the bead. Unlike the FV scheme, the boundary conditions are located at the edge of the cells and nodes j=1 and j=S are within. Consequently, the expressions at these nodes were treated differently from the FDS as the boundary conditions are held on the border of the cells. The first gird point j=1 is in cell $v_{a,1}$ where its left boundary is the edge of the center (as shown in figure 3.3). Hence, a fictitious point was applied to manage the applicability of

the node. Moreover, the left total flux $J_{\mathrm{tot,L}}(1\,,\mathrm{t_m})$ was set to zero. So, the molecules of all species were moving in the right direction.

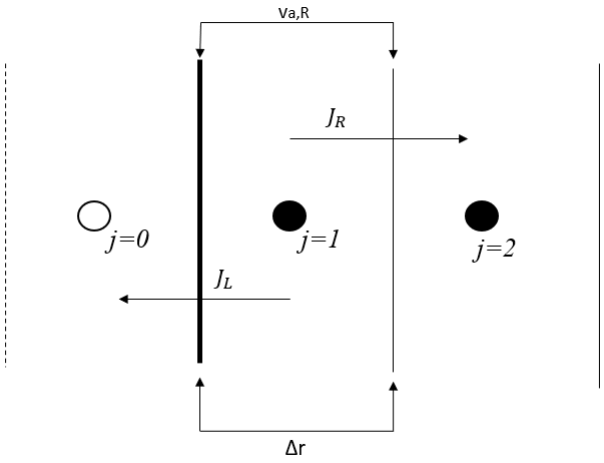

Figure 3.3 Schematic of Node j=1 in the Cell $v_{a,1}$ which is located close to the Center. J_L was set to zero since no flux exhibited at the left boundary of the cell.

Then, the mass balance at j=1 becomes

$$\frac{\partial C_i}{\partial t}(1, t_m) = -3\frac{J^R_{tot,i}}{\Delta r} \tag{3.2.8}$$

Where the flux at the right side can be integrated over cell $v_{a,1}$. The application is different on the surface of the sorbent. J_{total} was validated at cell $v_{a,S}$ to allow neutral species to leave the system, such as CO_2 or H_2O, and create a concentration gradient. Since the surface of the cell was exposed to the surrounding, the right boundary was set to a concentration of species i as illustrated in figure 3.4. Hence, the concentration at the right boundary of cell $v_{a,S}$ can be written as the averaged value of the neighboring grid points.

$$C_{R,i} = \frac{C_i(R,t_m)+C_i(R+1,t_m)}{\Delta r} \tag{3.2.9}$$

Where $C_{R,i}$ is the concentration of species i that was obtained from the surface reactions

(equations 2.2.14 and 2.2.16). Thus $C_i(R+1, t_m)$ was solved based on known concentrations at t_m that was found previously. Finally, the mass balance at j=S becomes

$$\frac{\partial C_i}{\partial t}(S, t_m) = -\left[\frac{J^R_{tot,i} - J^L_{tot,i}}{\Delta r} + \frac{J^R_{tot,i} + J^L_{tot,i}}{r_S}\right] \qquad (3.2.10)$$

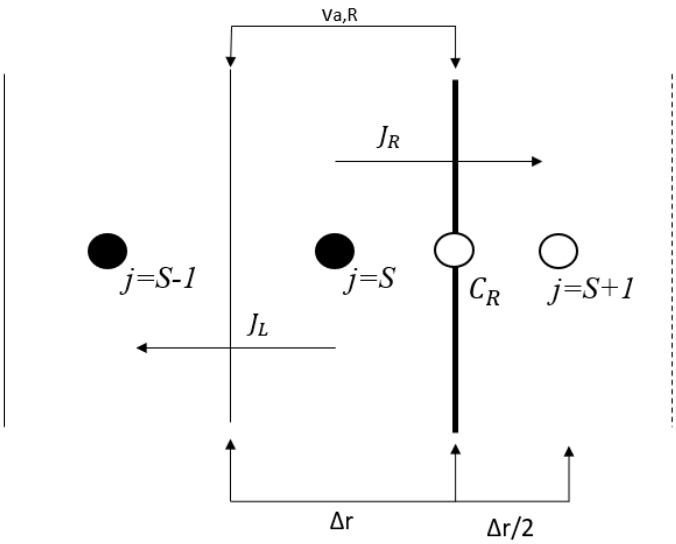

Figure3.4. Schematic of j=S which is Located Close the Surface of the Bead.

FV scheme was expressed at each node inside 1-D spherical domain. With the assumption of constant D_i and μ_i, the equilibrium reactions occur spontaneously depending on the initial concentrations at each node. The approximated mass balances of species concentrations (HO^-, HCO_3^-, CO_3^{2-} and H_2O) were simulated using MATLAB to obtain the temporal-spatial evolution over [0, R]. Also, $P_{CO_2}^{t_m+1}$ was determined to understand the behavior of an arbitrary sorbent with specific conditions that were originally set. Moreover, mass conservation was applied to examine the validity of the scheme.

3.3: ARBITRARY ISOLATED ABSORPTION SYSTEM

The finite volume and difference schemes that have been employed in spherical geometry, must accommodate moisture swing sorbent specific conditions to obtain the internal change of species concentrations; estimate CO_2 uptake rate and test other parameters. Hence, the simulation was based on arbitrary spherical sorbent. The system consists of an isolated chamber that has constant temperature and pressure and a sorbent placed in the middle of the chamber (figure 3.4.1). The sorbent then was exposed to an ambient air at known P_{CO2} and P_{H2O} to manage the process of absorption and desorption cycles of the sorbent. This methodology supported the sets of conditions that have been made and assisted in achieving a conservative outcome.

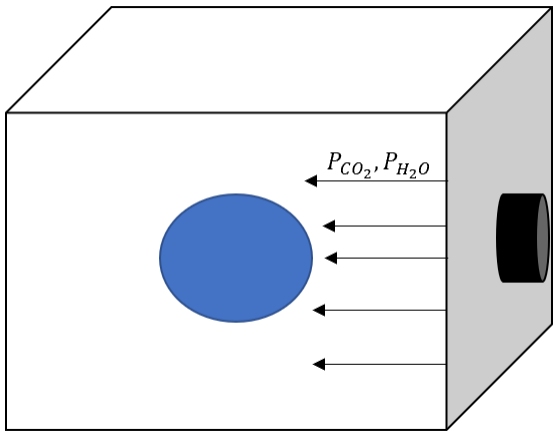

Figure 3.5. Basic Schematic of the Model Used in the Simulation. The bead was Installed in the Middle of The Chamber and Exposed to P_{CO2} and P_{H2O}.

The configurations of the spherical bead and the chamber were considered constant to reduce the number of variables in the simulation. The radius of the bead was the same

size as the one used in the previous model, which was equal to R=600µm. The chamber size was set with respect to the size of the bead to enhance the exposure of the air to the bead. So, the chamber size was $1x10^{-5}$ m^3 and so the air (V_{air}) inside the chamber. The only known concentration of cation inside the sorbent was NR_4^+=1620m^3/kg.[5] The cation concentration was considered to be evenly distributed across the shells of the sorbent to satisfy electroneutrality assumption and account for the presence of the anions.

For initial concentrations of HO^-, HCO_3^-, CO_3^{2-} and H_2O, local equilibrium was applied at each shell and each species reached equilibrium at initial conditions prior to varying the surrounding air content. As mentioned before, equilibrium constant K_2 of reaction $HCO_3^- + HO^- \overset{K_2}{\leftrightarrow} CO_3^{2-} + H_2O$ is dependent on the local moisture content and can shift the equilibrium reaction when adjusting C_{H2O}. Moreover, since the surface of the bead can be modified into either hydroxide or carbonate phase, it was assumed that the initial phase of the sorbent was carbonate with $x \geq 0.5$. That helped avoid undefined solutions due to the nature of the schemes. The diffusion coefficients were specified at low rate to accommodate the nature of the polymeric resistivity and satisfy the actual values of concentrations. The parameters became 5.3x10^-9m^2/s, 1.2x10^-9m^2/s, 0.9x10^-9m^2/s and 9.2x10^-10m^2/s for HO^-, HCO_3^-, CO_3^{2-} and H_2O, respectively (Zeebe, 2011). On the surface of the sorbent, P_{CO2} and P_{H2O} were controlled parameters to examine multiple schemes. For $P_{CO2,}$ the value ranged between 300-650ppm. On the other hand, water concentration was controlled by varying relative humidity of the air from 5%-80%. Both parameters would alter the conditions over the surface of the bead and hence the fluxes would trigger the reactions and create a concentration gradient inside the sorbent.

To validate the numerical models and maintain consistency with MSA, some assumptions have been considered to provide global and local boundaries in the system:

- The global temperature and pressure of the whole system were constant.
- The partial pressure of CO_2 and RH were controlled at known values and kept constant in the whole system. With that being said, the mass of carbon and water was conserved within the chamber.
- The diffusion coefficients were constant and uniform across the whole domain of the bead [0,R].
- Ionic mobility coefficients of the ions were set equal to diffusion coefficients for simplicity purpose.
- The initial concentrations $C_i(r_{j,}0)$ were obtained based on the initial conditions of $P_{CO,}$ water content inside and above the surface and equilibrium constant.
- The ions: HO^-, HCO_3^- and CO_3^{2-} and H_2O were the only mobile molecules inside the bead and NR_4^+ was immobile and bonded to the shells.
- The fluxes inside the beads were between the grid points of FD scheme and the cells of FV scheme.
- Total species fluxes were null over domain [0,R].
- The generic mass balance of diffusion-drift-reaction equations were assumed to allow the present molecules undergo a twostep process: first, fluxes shift the molecules along $0<r_j<R$ to next time step t_m, then local equilibrium readjusts the concentrations.
- Carbon dioxide was considered as the total carbon inside the system $\Delta Carbon = C_{HCO_3^-} + C_{CO_{3^{2-}}}$. The initial mass of carbon prior to adsorption was subtracted.

In order to evaluate all the assumptions made and the constructed schemes, MATLAB simulator was utilized to examine a number of expectations which will be discussed in the next chapter. Thus, the numerical procedures for FDS and FVS were as the following: P_{CO2} and P_{H2O} of the system were adjusted, then internal concentrations went out of equilibrium and started to evolve toward new surface boundary conditions. C_i at for each species were evaluated at t_{m+1} through the mass balance equations

$$C_i(r_j, t_{m+1}) = C_i(r_j, t_m) - \Delta t \left[\nabla J(r_j, t_m) + \frac{2}{r} J(r_j, t_m)\right]$$

Knowing that equilibrium reactions occurred instantaneously which can be solved through equilibrium relationship

$$K_2 C_{CO_3^{2-}}(r_j, t_{m+1}) C_{H_2O}(r_j, t_{m+1}) - C_{HO^-}(r_j, t_{m+1}) C_{HCO_3^-}(r_j, t_{m+1}) = 0$$

3.4: CO_2 EQUILIBRIUM AND WATER ISOTHERM CALCULATIONS

To converge into additional useful outcomes from the built FV model, MSA had to be examined through multiple approaches. Saturation of CO_2 (θ), CO_2 uptake capacity (q_e) and absorption equilibrium constant (K) were determined by imposing Langmuir isotherm. The thermodynamic relationship of the gas-solid interaction expresses the uptake rate of CO_2 by the bead and the equilibrium rate at which absorption was occurring (Lackner et al., 2011). Then isotherm can be identified by the following equation 3.4.1.

$$\frac{1}{q_e} = \frac{1}{K q_\infty} \frac{1}{P_{CO_2}} + \frac{1}{q_\infty} \qquad (3.4.1)$$

Where q_∞ is CO_2 absorption capacity. The equation was solved through varying P_{CO2} iteration to obtain several values of q_e. After the sorbent reached saturation, CO_2 uptake capacity was calculated to estimate the equilibrium absorbed gas.

$$q_e = n_{initial} + n_{CO2} - \Delta Carbon_{final} \quad (3.4.2)$$

Where $n_{initial}$ is the initial amount of carbon inside the bead, n_{CO2} is the initial amount of CO_2 that was controlled in the system and $\Delta Carbon_{final}$ is the total amount of carbon inside the bead after reaching absorption equilibrium. Consequently, the values of P_{CO2} and q_e were fitted into equation 3.4.2 to obtain the intercept and the slope of the linear line.

In addition, the variation of RH was studied to examine how water vapor perturbs q_e and minimizes the equilibrium absorption of the bead. If the hypothesis on CO_2 saturation reduction could be confirmed, then the numerical scheme used (FVM) with the applied conditions should show carbon shift and reduction due to water concentration gradients. The linear equilibrium relation of water above and on the surface (eq: $C_{R,H_2O} = k_{H_2O}P_{H_2O}$) states that partial pressure of water above the surface can be directly integrated into C_{H2O}. However, this is not true all the time especially in polymeric absorption. Water molecules behave differently on sorbent surfaces and tend to have a nonlinear relationship (Wang et al., 2017). Yet, there is no specific isotherm that describes water behavior accurately. Therefore, Freundlich isotherm was utilized in the recent study assuming the water non-linearly equilibrates on the surface as shown in equation 3.4.3.

$$C_{R,H_2O} = k\left(P_{H_2O}\right)^p \quad (3.4.3)$$

Where k and p are experimental parameters. There are no specific values from the previous parameters, but it was recommended to use p>1 in order to accomplish MSA absorption. Moreover, k could be evaluated using the magnitude of Henry's constant H`=3.3x10^{-3} of CO_2. Hence, it was assumed that k is higher than H'_{CO2}. Both the linear and non-linear isotherms were conducted to estimate C_{H2O} and obtain moisture effect on q_e of CO_2 in the sorbent.

P_{CO2} was changed above the sorbent to examine the change in water content inside the bead. This uncommon scenario was applied to check if the total change in C_{Carbon}, resulting from increasing P_{CO2}, could drive water molecules out and decrease total ΔC_{H2O} (as expressed in equation 3.4.5). Also, C_{H2O} values, located at node j=1 (close to the center) and node j=R (close to the surface), were plotted to identify the effect of varying C_{Carbon} on C_{H2O} at these gird points.

$$\Delta C_{H_2O} = \sum C_{H_2O,initial} - \sum C_{H_2O,final} \qquad (3.4.5)$$

CHAPTER 4

RESULTS

In this section, the outcomes from the previous constructed methodology will be presented. The results section will introduce and discuss the outcomes of FDS and FVS temporal-spatial evolution of species concentration, the absorption/ desorption cycles and CO_2/H_2O isotherms evaluations.

4.1: NULL FLUXES AT CENTER BOUNDARY CONDITION IN FDS

Through the finite difference method, the mass balance equation 2.2.19 of species HO^-, HCO_3^-, CO_3^{2-} and H_2O at each shell r_j of the sphere was approximated explicitly to determine C_i at $t_m+\Delta t$. The approximated equations were solved dependently based on known initial concentrations of all species at 3 nodes $[r_{j+1} - r_j - r_{j-1}, t_m]$. At each node r_j, All molecules were sharing the same space at the same time. Since it was assumed that the nature of the sorbent (which was arbitrary) was sensitive to the surrounding, C_i at all nodes $0<r_j<R$ were determined at $t_m=0$ when sorbent reached equilibrium state at P_{CO2}=200ppm, RH=5%. Therefore, the system conditions could be altered to observe the temporal-spatial evolution of all species while accounting for the two-stage process.

To carry a consistent mass balance equation, the size of intervals Δr and Δt had to be uniform over the total time t (t=200s) and total space ($R=6x10^{-4}m$) of the simulation. Moreover, G should be less or equal to 0.5 to avoid instability when solving four approximated concentration equations. The following figures 4.1 and 4.2 illustrate the concentrations of HCO_3^- and CO_3^{2-} along time and space [0, R], [0, t].

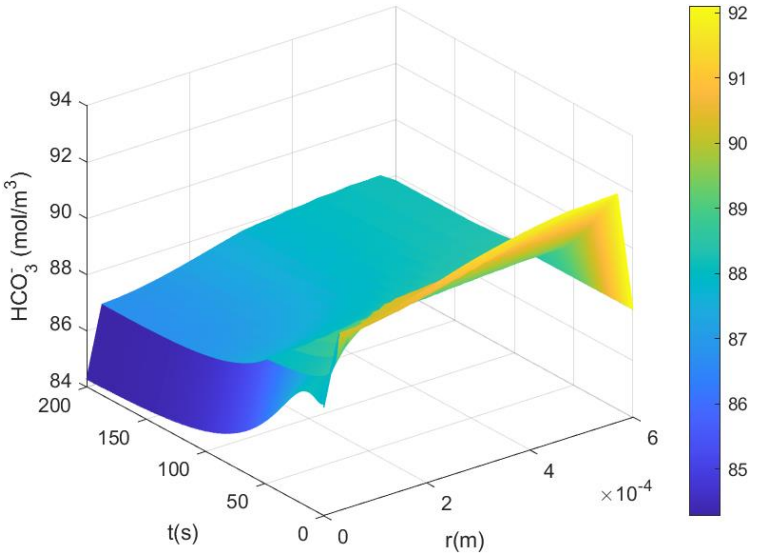

Figure 4.1. Bicarbonate Concentration Change over space and time applying FDS. x-axis Represents Radius of the Sphere in Meters and y-axis is Time in Seconds. The right bar represents the concentration intensity.

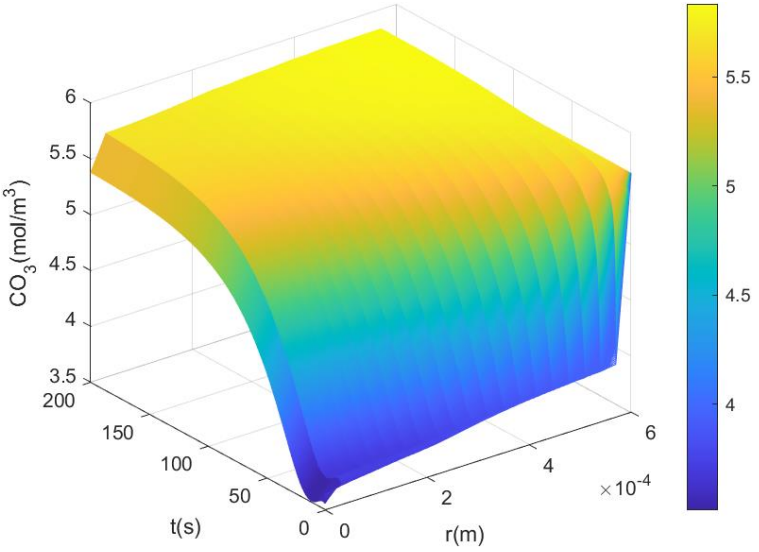

Figure 4.2 Carbonate Concentration Change over space and time applying FDS. x-axis Represents Radius of the Sphere in Meters and y-axis is Time in Seconds. The right bar represents the concentration intensity.

Carbonate and Bicarbonate began evolving inside the intervals due to altering

equilibrium reactions above the surface. As P_{CO2} changed to 400ppm and P_{H2O} at 15%,

the equilibrium reactions and electroneutrality readjusted all species concentrations. Hence, the flux gradients started to promote molecules movement over internal nodes. As shown in previous figures, carbonate and bicarbonate concentrations were approaching steady state at the end of the simulation time. Thus, the molecules approached equilibrium stage of internal reactions and $C_i(r_j, t_m)$ and $C_i(r_j, t_{m+1})$ difference decreased over time. Moreover, after varying P_{CO2} and P_{H2O}, $C_{HCO_3^-}$ decreased and $C_{CO_3^{2-}}$ increased gradually over time indicating a shift occurring at equilibrium reactions at the surface and within the shells. On the other hand, there were no significant alterations over the edges, neither on the surface (constant concentrations) nor at the center (zero fluxes as Robin BC identified). Additionally, The results showed a similar behavior to Remy's simulation (2014) which indicated that the species concentrations were independent of space and time.

At the surface side of the sorbent, the amount of CO_2 was subject to change since the model was assumed to have a constant volume of the gas in the system. Furthermore, the surface of the sorbent experienced fluxes in both directions that maintained a consistent change in P_{CO2} until the sorbent reached global equilibrium along all spatial nodes. Therefore, to assist in the numerical analysis and confirm CO_2 uptake, absorption and desorption cycles of P_{CO2} (in unit part per million) have been conducted based on fixed boundary conditions. Also, to visualize how Neumann BC could alter the solution, the absorption/desorption cycles of the perspective scheme were incorporated along the study. Desorption relative humidity RH was set at higher values than the absorption RH conditions. Hence RH of 75% was employed at the saturated bead. The following figures 4.3 and 4.4 visualize the absorption desorption cycles of P_{CO2} when using Neumann and

Robin boundary conditions, respectively. The partial pressure was estimated at each time step using equation 2.3.6.

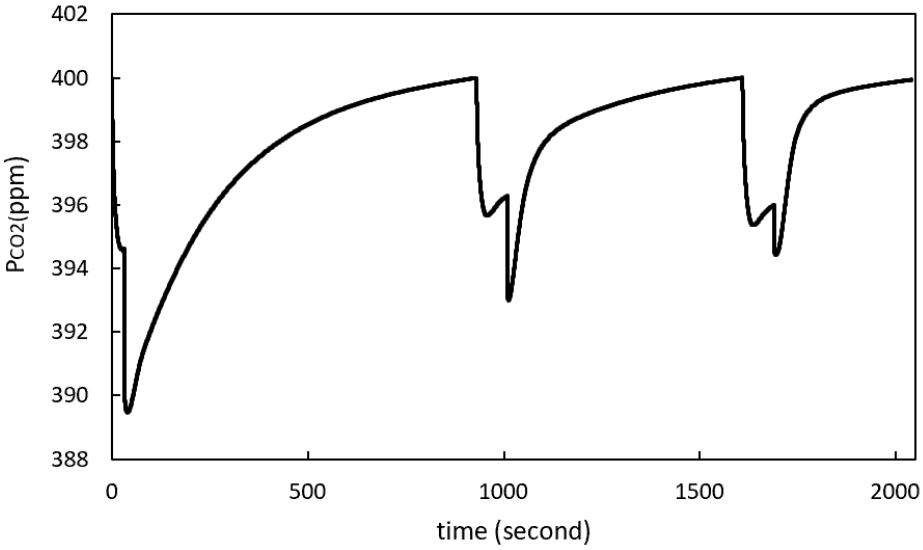

Figure 4.3 CO2 Absorption Desorption Cycles Above the Sorbent Surface When Appling Neumann BC in FDS.

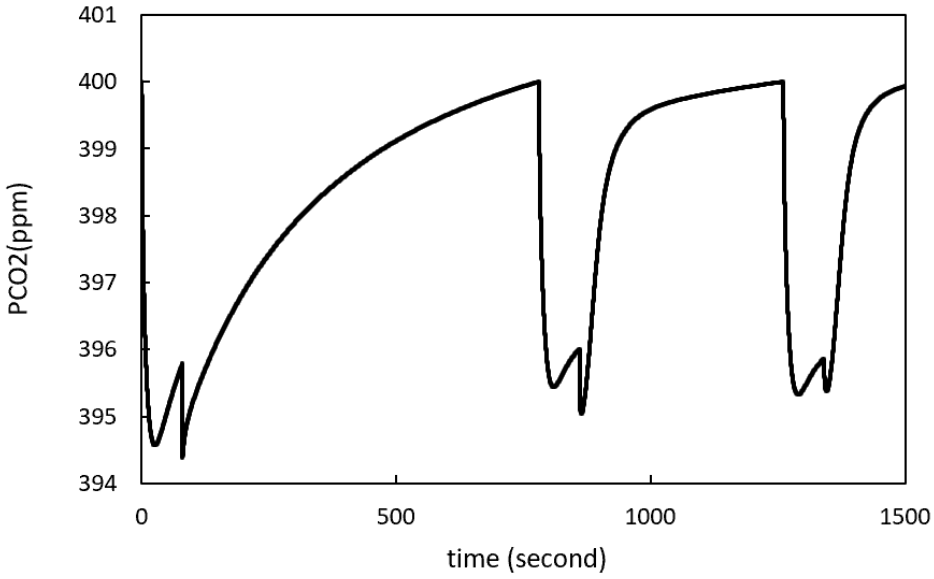

Figure 4.4 CO2 Absorption Desorption Cycles Above the Sorbent Surface When Appling Robin BC in FDS.

The absorption process started at P_{CO2} 400ppm with RH=15%. Then once the sorbent reached saturation (the lowest part in the graphs) the RH of the air was readjusted to RH=75% in order to release CO_2 from the bead. As illustrated in both figures, three cycles have been simulated. The first cycle experienced longer desorption time than the other two cycles. The reason was due to the mass conservation. As both schemes gained mass in the first cycle, they were adjusted using carbon mass conservation in previous model (equation 2.3.5). Hence, the duration cycles and absorbed amount were fixed after employing the mass conservation equation.

When applying Neumann or Robin BC, the saturation stage did not show stability of CO_2 uptake. Consequently, the simulation did not converge to a certain equilibrium value of P_{CO2}. That's due to the continuity of concentrations gradients for HCO_3^- and CO_3^{2-} between the surface and the surrounding. On the other hand, the carbon mass gain of FDS that was incorporated by Neumann and Robin BC was 1.96% and 1.85% of the original mass $n_{intital}=6.6022x10^{-7}$mol, respectively. Hence, with the slight reduction of mass gain by Robin BC, the scheme was still susceptible to mass loss or gain. That could be explained by two possible reasons: Finite difference method in general does not conserve mass within a certain domain which may cause loss or gain in mass through factors other than the boundary edges; or the internal nodes with the node at the center should be treated implicitly to verify the concentrations of each species at r_j and t_m without considering next t_{m+1} evolution.

4.2: STUDY OF FINITE VOLUME SCHEME

Finite volume scheme was the alternative simulation that was expected to conserve mass and reduce instability in the outcomes. As FVS discretized the intervals into cells, the nodes were still considered as the base of all concentrations. The mass, as the scheme stated, is conserved within each cell v_a, whereas the averaged concentrations are located at the nodes j=1, …, S. Hence, in the following section, the temporal-spatial evolutions of HCO_3^- and CO_3^{2-} were evaluated at every single gird. The absorption/desorption cycles of P_{CO2} were then obtained and carbon mass loss was estimated.

For consistency, the procedure for changing the surrounding conditions was the same. The absorption conditions were P_{CO2}=400ppm and P_{CO2}=15%. The tested domain partitioned into S=20 and M=80 gird points for simulation. The next figures 4.5 and 4.6 show the simulation outcomes of species mass balances.

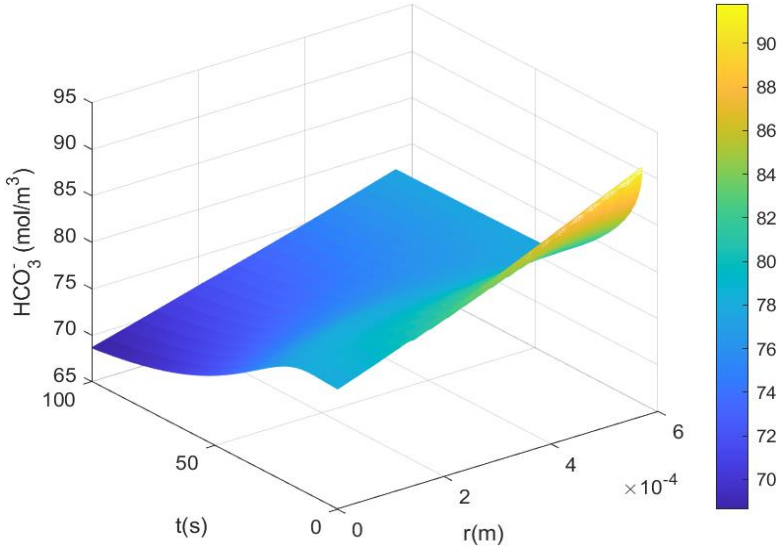

Figure 4.5 Bicarbonate Concentration Change over space and time via FVS. x-axis Represents Radius of the Sphere in Meter and y-axis Represents Time in Seconds.

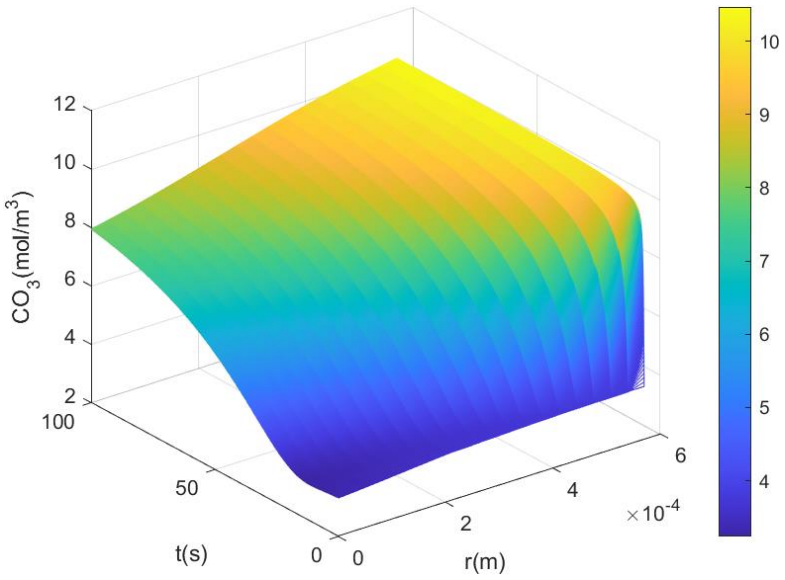

Figure 4.6 Carbonate Concentration Change over space and time via FVS. x-axis Represents Radius of the Sphere in Meter and y-axis Represents Time in Seconds.

Both figures show that the carbon species were derived via changing the concentration of CO_2 and H_2O in the surface of the sorbent and species concentrations at the surface $C_{i,R}$. Both species evolved from the initial concentrations when the bead is not at equilibrium state (at t_m=1) to reach steady state at the end of simulation time. Once the change of $C_i(r_j, t_m)$ and $C_i(r_j, t_{m+1})$ approached low mass fraction change ($\Delta C \leq 0.1\%$) at a random grid point j, the simulation stopped. Bicarbonate and carbonate concentrations equilibrated faster at nodes that are closer to the surface than the center. The species concentrations at the surface (HO^-, HCO_3^-, CO_3^{2-} and H_2O) were implemented directly into the approximated equations of mass balance. Therefore, the gradients adjusted the neighboring nodes that contained all species concentration to equilibrate at t_{m+1}. Moreover, the node at the center (j=1) did not experience a significant change since it was solely dependent on the right diffusion drift flux. In fact, the concentrations were

dependent on the time and space interval as they experienced change over time to reach global equilibrium.

Following the same procedure conducted in the previous subsection, CO_2 absorption desorption would be determined via calculating P_{CO2} using equation 2.3.6. In the end of each time step from the approximated mass balance, P_{CO2} was updated. The next graph shows the absorption/ desorption cycles over period of 500 seconds inside a simulated arbitrary system.

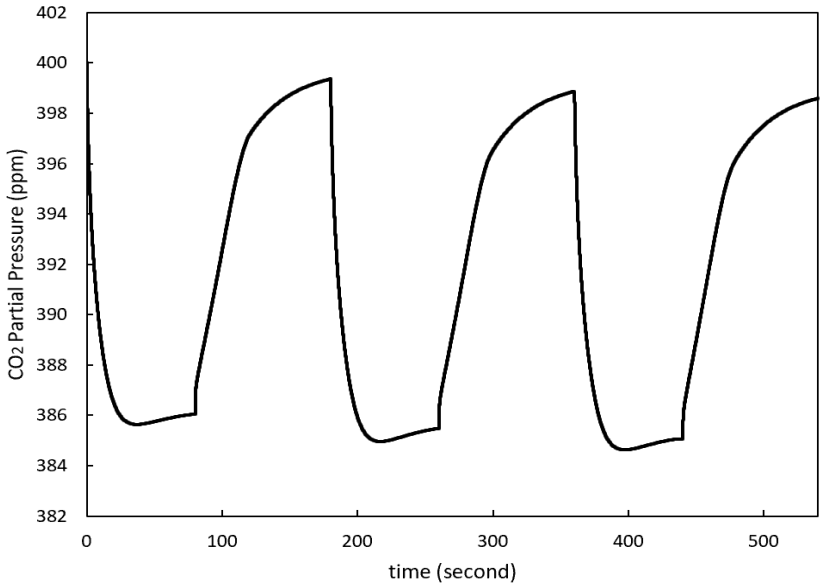

Figure 4.7 CO_2 Absorption Desorption Cycles Above the Sorbent Surface applying FVS.

The simulation produced significant results. The total time of all three cycles in FVS is shorter than in FDS. This is due to the original simulation of FVS at which it reached saturation in shorter period than expected. Moreover, the equilibrium P_{CO2} was 385ppm once the sorbent reached saturation. The trend emphasized that the saturation level and desorption plateau were partially stable as there were no sudden changes of P_{CO2}. The

desorption reached plateau that designates the release of CO_2 and sorbent global equilibrium state. Furthermore, the simulation was not modified by the mass conversation equation to adjust mass gain or loss since the results showed a flat saturation and desorption plateau trend over three cycles. Accordingly, the mass loss from the original amount C_{carbon}= 6.6022x10^{-7}mol was 0.3% which was a reasonable error if globally accounted in the system. Hence, FVS proved its potential in applying effective conservative approximation model to evaluate the diffusion-drift-reaction equations for MSA and sustain CO_2 saturation and desorption.

The sorbent tended to preserve more carbon than releasing it which was another outcome that was detected in the cycles previously. The total carbon inside the sorbent after 1st, 2nd and 3rd absorption was 6.24x10^{-8}mol, 6.26x10^{-8}mol and 6.27x10^{-8}mol, respectively. Thus, the saturation level line in figure 4.7 decreased slightly after each cycle period.

4.3: CO_2 AND WATER ISOTHERM ANALYSIS

Carbon dioxide and water isotherms were additional factors that have been applied to integrate the outcomes and validate the performance of the sorbent using FVS. The absorption phase in the simulation assisted in obtaining the CO_2 absorbed at equilibrium (q_e) at different controlled values of P_{CO2}, and then fitting them into Langmuir isotherm to obtain q_∞ and K. Later in this subsection, varying values of P_{CO2} and P_{H2O} were employed to observe the behavior of the uptake rate of CO_2 and water content inside the sorbent. Also, two water isotherms were simulated to detect the discrepancies between them when calculating CO_2 saturation θ.

To satisfy Langmuir curve, the simulation had to run several values of P_{CO2} equilibrium in order to obtain q_e. Hence, the values were fitted in the isotherm as $\frac{1}{P}$ vs $\frac{1}{q_e}$, from which the slope and intercept ($\frac{1}{q_\infty}$) were found. The calculations were made at constant RH over the sorbent and the sorbent has to reach global equilibrium. The following figure 4.8 plots the isotherm curve at P_{CO2} =300-650ppm.

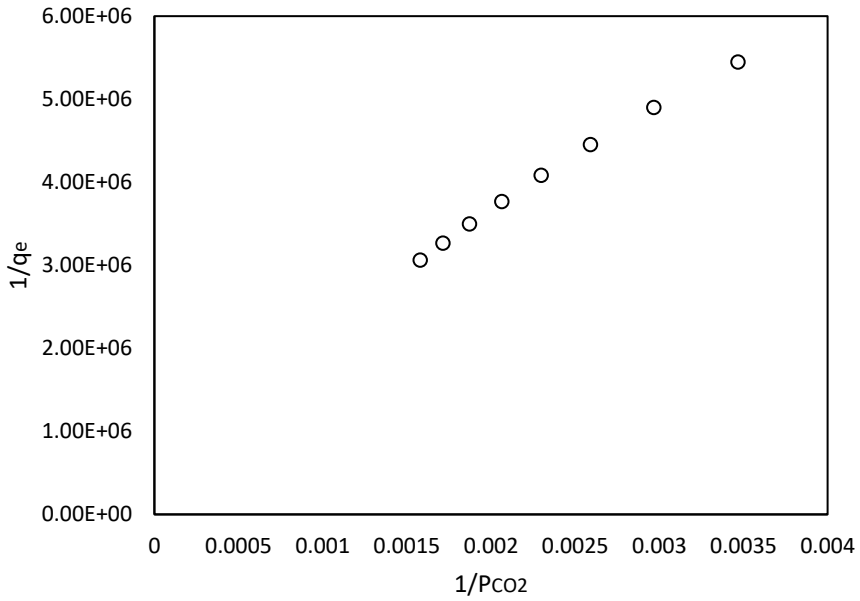

Figure 4.8 Langmuir Isotherm Curve of Several values P_{CO2}. q_e in mole and P in ppm.

The calculated q_e was in the magnitude of power -7, so $1/q_e$ on the y axis, was in the magnitude of power 6. The high partial pressure of CO_2 at 650ppm led to an increase in absorbed CO_2 ($3.27x10^{-7}$mol) at equilibrium. Whereas the lowest amount absorbed was at 300ppm. Hence, there was a proportional relationship between P_{CO2} and q_e at constant RH. q_∞ from the curve was obtained at $8.26x10^{-7}$mol which was and hence $K=8.02x10^{-4}$. To further asses the model, two scenarios were considered through either varying P_{CO2} or P_{H2O} to determine their effect on the sorbent. Increasing RH was expected to decrease

CO_2 saturation in the bead at constant P_{CO2}. On the other hand, C_{H2O} inside the bead was examined at varying P_{CO2} and constant P_{H2o}. The results would provide an insight on the effect of varying CO_2 molecules on the original water content.

The following figure 4.9 shows the calculated values of CO_2 saturation (θ) inside the bead with respect to RH% of the system [RH=15%-75%]. The water isotherms (linear and nonlinear) were applied in the study to visualize the discrepancy that could occur if water equilibrium behaved differently over the surface. Hence the linear equation $C_{R,H_2O} = k_{H_2O}P_{H_2O}$ and the nonlinear equation $C_{R,H_2O} = k\left(P_{H_2O}\right)^p$ were considered at the boundary of the surface. The isotherm unitless parameters k and p were estimated knowing that p>1.

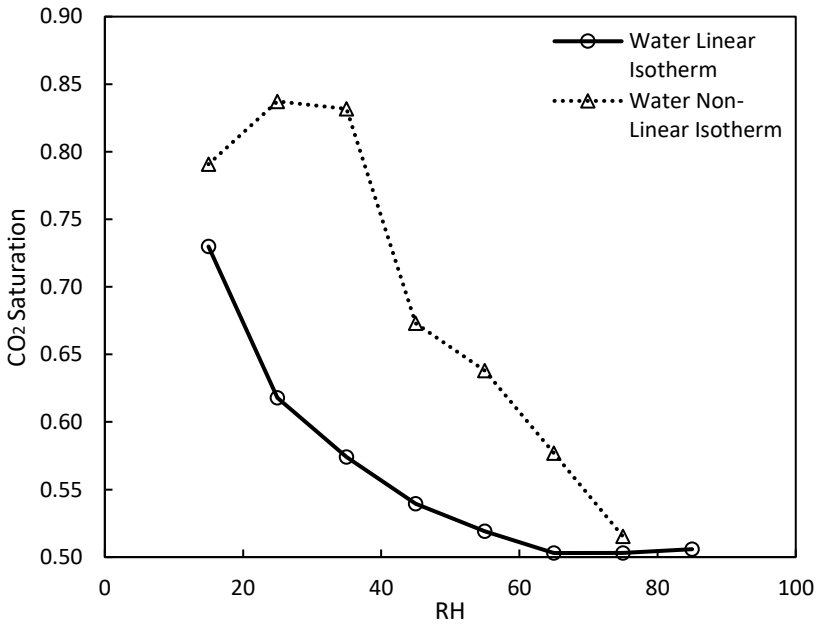

Figure 4.9 CO_2 Saturation θ When increasing RH% of the System. Two Trend Lines were Added for Water Isotherms.

The figure herein shows that increasing RH of the air reduces the CO_2 saturation in the sorbent for both linear and non-linear water isotherm. θ was adjusted above 0.5 since it

was assumed that the total carbon already existed at initial stage of sorbent. The saturation dropped from 0.85 to lower than 0.55 which indicated that water presence at high humidity level inhibits CO_2 uptake absorption and reduces the available reactive sites that binds with the gas. While the calculations were conducted under two water isotherms, the linear relationship which was assumed by Remy and Robin showed a significant decline in θ and then stabilized at high RH. Hence, C_{H2O} was directly affecting CO_2 saturation. Unlike with the nonlinear isotherm, namely Freundlich isotherm, the results were fluctuating at RH below 50% and decreased significantly at higher RH. Yet, Freundlich isotherm did not describe the actual behavior of water at the surface that was observed in the experimental study by Lackner and coworkers (2011) Resin I-200 showed a gradual decrease of θ when increasing water vapor up to10ppt and considerable θ drop at higher water vapor (greater than 10 ppt).

FVS was simulated again at inverse conditions. The new model is based on a constant RH and varying P_{CO2}. The next figure 4.10 illustrates P_{CO2} effect on ΔC_{H2O} which was estimated from equation 3.4.5.

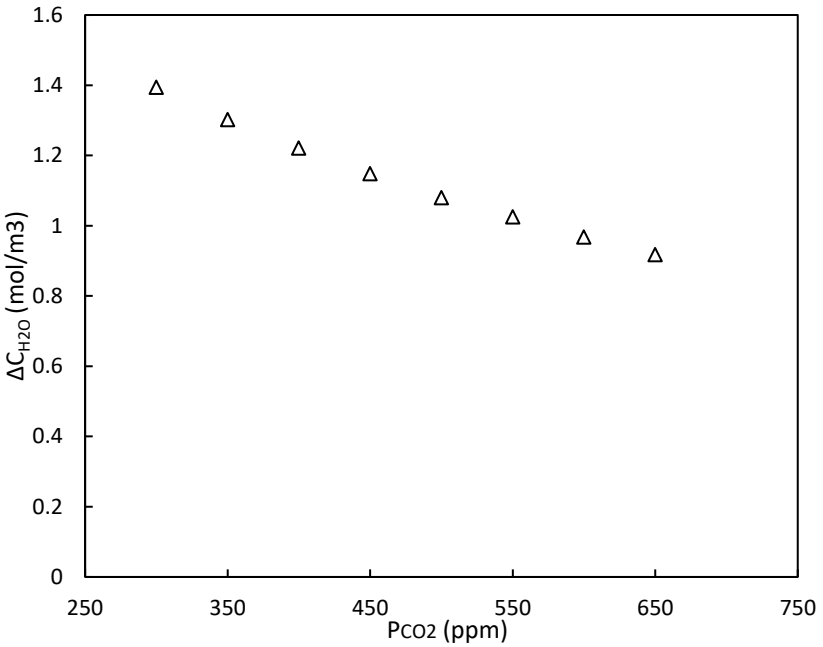

Figure 4.10 CO_2 Partial Pressure Effect on the Presence of Water Inside the Sorbent.

The total amount of water was estimated based on its initial presence in the bead and after the sorbent reached global equilibrium. As the P_{CO2} was increasing, the equilibrium reactions on the surface destabilized and reached a new local equilibrium level. The total amount of water was decreasing. Carbon inside the bead maintained its presence at high concentrations which drove water molecules out of radii domain [0, R]. Furthermore, a significant observation from FVS simulation was indicated at internal grid points j=1, …, 20 as shown in the figure 4.11.

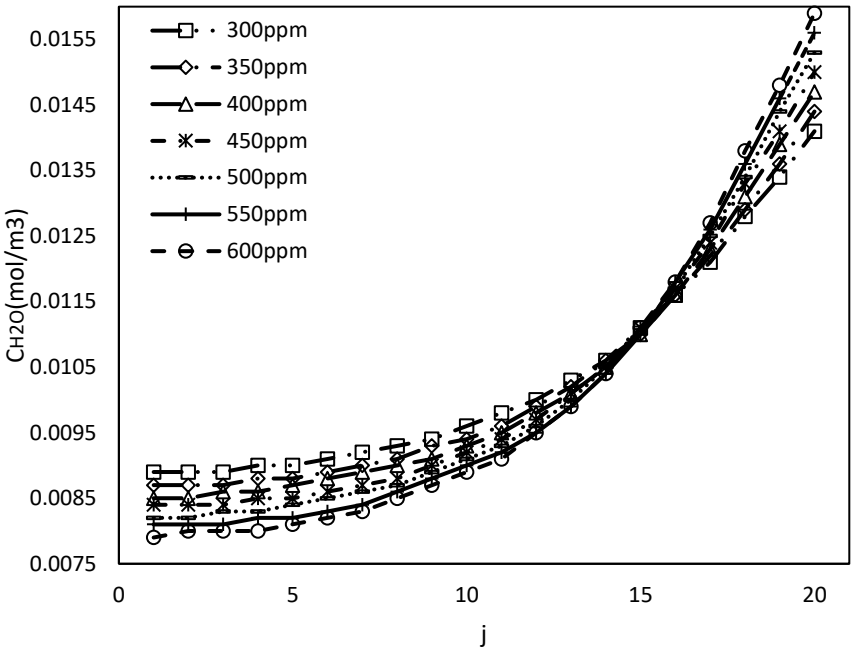

Figure 4.11 CO_2 Partial Pressure Effect on Water Concentration at Internal Grid Points.

At gird points that were closer to the center, C_{H2O} was gradually decreasing as the P_{CO2} increased to 600ppm. In contrast, at nodes closer to the surface, C_{H2O} experienced an incline when varying P_{CO2} to higher level. That explains C_{H2O} gradients direction which was toward the surface. Water molecules were intending to leave the surface of the bead after increasing the presence of carbon. Theoretically, MSA equilibrium reaction, $HCO_3^- + HO^- \overset{K_2}{\leftrightarrow} CO_3^{2-} + H_2O$ shifts to the right as drier the sorbent becomes inside. Consequently, higher absorption capacity at higher P_{CO2}.

CHAPTER 5

CONCLUSION AND FUTURE RECOMMENDATIONS

In summary, moisture swing absorption had been proposed by Lackner (2011) in previous experimental setup. The mechanism shows the ability of a polymer to absorb CO_2 when dry and release it when wet. Then, Remy and Robin conducted extensive theoretical and experimental procedures to understand the numerical model of MSA. Approximation scheme was utilized to model the diffusion-drift-reaction equations of HO^-, HCO_3^-, CO_3^{2-} and H_2O and discretize the domain of the sorbent's geometry. The goal of the study is to fix the original scheme at the boundary through applying Robin boundary condition to restrict ions mobilization to the other side. Alternatively, finite volume method was imposed to obtain lower carbon mass loss or gain within the simulation. Lastly, the isotherm parameters were determined and studied to evaluate the performance of the simulation.

More studies should be conducted to develop a more effective and high-resolution MSA simulation. Since the mass balance of species concentrations show other species concentrations as dependent variables, making the model simultaneously approachable, iteration coefficients can be considered to increase the accuracy of the simulation outcomes. The method could be extremely expensive since there are 4 dependent species, but it could offset the numerical barriers in future studies when applying real sorbents. Furthermore, the model can be scaled up to a packed bed system. The simulated MSA filtration system could predict the total uptake rate of the system and optimize the best conditions to accommodate real life projects and experiments.

In addition, the equilibrium constants of MSA reactions could vary based on the moisture level and the type of resin used in the study. Thus, it is recommended to conduct theoretical and experimental thermodynamic models that signify a relationship between the equilibrium constants (K_1 and K_2) and water contents within sorbent configurations. In addition, determining experimentally the released heat from moisture absorption operation can clarify the relationship of the surface with surrounding water vapor.

REFERENCES

Okai, W. Delmotte, V. Portner, H. Skea, J. Pirani, A. Pidcock, R. Chen, Y. Lonnoy, E. Connors, S. Zhou, X. Maycock, T. Tignor, M. Zhai, P. Roberts, D. Shukla, P. Pean, C. Mathews, J. Gomis, M. Waterfield, T. (2018). Global warming of 1.5°C. Retrieved from *chromeextension://cefhlgghdlbobdpihfdadojifnpghbji/https://www.ipcc.ch/site/assets/uploads/sites/2/2019/06/SR15_Full_Report_High_Res.pdf*

Berger, A. Bhown, A. (2011). Comparing physisorption and chemisorption solid sorbents for use separating CO2 from flue gas using temperature swing adsorption. *Energy Procedia, 4, 562-567.* Retrieved from https://www.sciencedirect.com/science/article/pii/S1876610211000919

Wang T. Lackner, K. Wright, A. (2011). Moisture Swing Sorbent for Carbon Dioxide Capture from Ambient Air. *Environmental Science and Technology, 45, 6670-6675.* Retrieved from https://pubs.acs.org/doi/10.1021/es201180v

Remy, I. (2014). Numerical Simulation of a Carbon Dioxide Pump. [Unpublished internship's report]. Columbia University

Robin, A. (2015). Modelisation and Calibration of moisture sensitive beads in Carbon dioxide capture. [Unpublished internship's report]. Arizona State University.

Mazumder, S. (2016). *Numericalmethods for partial differential equations finite difference and finite volume methods.* Waltham: Elsevier. Retrieved from https://www-sciencedirect-com.ezproxy1.lib.asu.edu/book/9780128498941/numerical-methods-for-partial-differential-equations

Wang, T. Hou, C. Ge, K. Lackner, K. Shi, X. Liu, J. Fang, M. Luo, Z. (2017). Spontaneous Cooling Absorption of CO2 by a Polymeric Ionic Liquid for Direct Air Capture. *The Journal of Physical Chemsitry Letters, 8, 3986-3990.* Retrieved from https://pubs-acs-org.ezproxy1.lib.asu.edu/doi/abs/10.1021/acs.jpclett.7b01726

Carbon Engineering (n.d.). Retrieved from https://carbonengineering.com/

ClimeWorks (n.d.). Retrieved from https://climeworks.com/

Zeebe, R. (2011). On the molecular diffusion coefficients of dissolved CO2; HCO_3^-,and CO_3^{2-} and their dependence on isotopic mass. *Geochemical Cosmochimica Acte, 75, 2483-2498.* Retrieved from https://ui.adsabs.harvard.edu/abs/2011GeCoA..75.2483Z/abstract

Patzay, G. (1995) A simplified numerical solution method for the Nernst-Planck multicomponent ion exchange kinetics model. *Reactive and Functional Polymers, 27, 83-89.* Retrieved from https://www.sciencedirect.com/science/article/abs/pii/138151489500